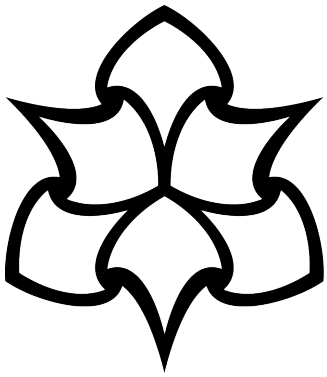

ADVANCED ENERGY MATERIALS
www.advenergymat.de

MoO_2 Nanowire Electrochemically Decorated Graphene Additively Manufactured Supercapacitor Platforms

Alejandro García-Miranda Ferrari, Jessica L. Pimlott, Michael P. Down, Samuel J. Rowley-Neale, and Craig E. Banks**

Additively manufactured (AM) supercapacitor platforms are fabricated from bespoke filaments, which are comprised of electro-conductive graphene (20 wt%) incorporated polylactic acid (80 wt%), via fused deposition modeling and denoted as G/AMEs. The G/AMEs are shown to be capable of acting as a template for the electrodeposition of metals/metal oxides, in particular MoO_2 nanowires (MoO_2-G/AMEs), which are subsequently explored as a capacitor within 1 M H_2SO_4, 1-butyl-3-methylimidazolium hexafluorophosphate, and 1-butyl-3-methylimidazolium tetrafluoroborate. Optimization of the MoO_2-G/AMEs demonstrates capacitance up to 1212 F g^{-1} when used in a symmetric arrangement. The material science described herein represents a significant enhancement in unlocking AMs potential as a valid manufacturing route for device level capacitance architectures.

1. Introduction

Additive manufacturing (AM) is a method of manufacturing in which a model designed by Computer Aided Design (CAD) is captured and subsequently constructed on a layer-by-layer basis. AM has become the preferential fabrication technology over more-classical manufacturing techniques, in certain niche applications, as it allows for the rapid transition from an initial CAD design to 3D objects. This is due to AM allowing for design considerations to be implemented without the restriction of only using 2D sheet components. At present, the technologies of AM are becoming increasingly capable and affordable, with much of the surrounding research focusing on the development of novel printing materials and the improvement of existing AM technologies; however, they are often still limited to producing inert/nonconductive 3D objects.[1] A potential route to expand the capabilities of AM to include the production of electro-active/conductive components requires enhancing AM feedstock's with electrically conductive printable composites for conductive pathway creation. However, this method is limited by its application of commercially available filaments, with only a few research groups capable of fabricating bespoke AM filaments for electrochemical applications. These developments provide integration of electronic components into AM designs, and even the AM of electronic components themselves.[2] The integration of 3D electronics in this manner is known as 3D structural electronics and allows electrical components to be designed to any form, providing a unique improvement over conventional electronics systems.[1c,3]

Supercapacitors, or electrochemical capacitors, have attracted a great deal of attention as energy storage devices since they have several advantages over batteries, such as high power densities, long life cycles, high reversibility, and relatively low cost. This makes them ideal for many applications, e.g., portable electronic devices, electrical vehicles, and emergency powers supplies.[4] Supercapacitors are used to be separated into two common categories: electrochemical double layer capacitors and pseudocapacitors. However, this latter notation has been explored demonstrating unambiguously that pseudocapacitance is incorrect and rather double layer charging and Faradaic responses are often superimposed.[5] The manufacturing of supercapacitors is typically accomplished by inkjet, screen-, and roll-to-roll printing, but recent advancements in AM have been shown this as a potential significant manufacturing approach for energy storage architectures.[6]

Foster et al.[6] demonstrated for the first time that the use of commercially available electrically conducting filaments can be utilized as freestanding anodes within lithium-ion batteries, by integrating graphene into a polymer matrix suitable for filament deposition modeling. In their study, a solid commercially available filament was used to demonstrate the potential of AM as an experimental approach to the development of energy storage architecture. This was the first demonstration of true AM to make electrodes for the application of energy storage. Down et al.[7] demonstrated that the approach could be used along with activate materials, integrated into the AM feed stocks, to fabricate a sodium ion full cell battery. Through integrating active materials into the filaments, the process of manufacturing energy storage architectures can entirely done by AM, with improved performance provided by an additional stage of post processing, through the partial dissolution of the polymer

Dr. A. García-Miranda Ferrari, Dr. J. L. Pimlott, Dr. M. P. Down, Dr. S. J. Rowley-Neale, Prof. C. E. Banks
Faculty of Science and Engineering
Manchester Metropolitan University
Chester Street, Manchester M1 5GD, UK
E-mail: m.down@mmu.ac.uk; c.banks@mmu.ac.uk

The ORCID identification number(s) for the author(s) of this article can be found under https://doi.org/10.1002/aenm.202100433.

DOI: 10.1002/aenm.202100433

Table 1. Comparison of various MoO_2-based supercapacitor composites.

Material	Fabrication methodology	C_s	Electrolyte and cell configuration	References
MoO_2-CC	Electrodeposition–hydrothermal	208 F g^{-1} (@3 mA cm^{-1})	1 M LiOH – asymmetric	[8]
MoO_2 nanorods	Thermal decomposition	140 F g^{-1} (@1 A g^{-1})	1 M H_2SO_4 – half cell	[9]
TiO_2/RGO/MoO_2	Hydrothermal	1636 F g^{-1} (@1.25 A g^{-1})	1 M H_2SO_4 – asymmetric	[10]
MoO_2	Hydrothermal	170.8 F g^{-1} (@1 A g^{-1})	1 M H_2SO_4 – half cell	[11]
MoO_2–graphene	Hydrothermal	355 F g^{-1} (@0.6 A g^{-1})	1 M Na_2SO_4 – symmetrical	[12]
MoO_2@C/CNT nanorods	Hydrothermal	1667.2 F g^{-1} (@1 A g^{-1})	3 M KOH – asymmetric	[13]
MoS_2/MoO_2@CNT	Microwave synthesis	228.4 F g^{-1} (@0.5 A g^{-1})	6 M KOH – asymmetric	[14]
NCs@MoS_2/MoO_2	Hydrothermal	569 F g^{-1} (@1 A g^{-1})	6 M KOH – half cell	[15]
MoO_2–rGO	Hydrothermal	356 F g^{-1} (@0.1 g^{-1})	6 M KOH – half cell	[16]
MoO_2-G/AME	AM–Electrochemical	1212 F g^{-1} (@1.48 A g^{-1})	$[C_4MIM][BF_4]$ – symmetrical	This work

matrix. Despite this, AM has not rendered studies of modifications and dopants on the surface morphologies to improve performance. This paper introduces additive manufactured electrodes (AMEs) as a platform for modification, with specific materials via electrochemical decoration, and explores their ability to perform towards energy storage applications; such modification requires an AME with a conducive surface that is only possible via bespoke fabricated conductive filaments, which are not commercially available. Note that the common approach in the literature is to buy in commercially available conductive graphene AM filaments, which are limited to a set low graphene % wt that limits its electrochemical conductivity and ability to be electrochemically modified. This limitation is overcome through the design and fabrication of bespoke highly conductive graphene AM filaments which are 20 wt%, reported herein. Transition metal oxides attract considerable attention in the field of energy storage, not only because of their beneficial reported mechanical, structural, or electronic properties, but due to their high capacitances associated with their multiple valence state changes, a trait not generally possible in carbon materials.[17] For example, molybdenum dioxide (MoO_2) with band gap of 3.85 eV has become a fascinating transition metal oxide because of the metallic electrical resistivity, high melting point, and high chemical stability. Its high density (6.5 g cm^{-3}) enables it to store more energy as supercapacitors with the same size of the battery compared with that of graphite (2.3 g cm^{-3}) anode-based batteries.[18] Comparative studies of MoO_2 and its supercapacitor performance have shown the material to have significant performance. Ju et al.[19] presented TiO_2/reduced graphene oxide (rGO)/MoO_2 composites, with a hierarchical nanostructure which have a capacitance of 1636 F g^{-1} at 1.25 A g^{-1}, highlighting the benefit of having an amorphous structure, such as the polymer matrix in this case, to supply more active site accessibility and facilitate the accommodation of volume expansion. Further to this Wu et al.[20] showed that the addition of a carbon structure increased the performance of MoO_2, whereas the presence of carbon nanotubes (10% wt) promoted the capacitive performance of MoO_2 from 327.4 to 424.7 F g^{-1}. **Table 1** provides a comparative summary of the state of the art of MoO_2 and the application in supercapacitor devices, showing capacitive performance from 140 to 1667 F g^{-1}. It should be clear that in the comparison of these papers, we are considering only the weight of the active materials of interest and are ignoring the presence of the inactive polylactic acid (PLA) binder, however we show that the electrochemical decoration with MoO_2 onto graphene additively manufactured electrodes (G/AMEs) can significantly increase the capacitive performance of the device.

Consequently, in this paper, we develop bespoke AM graphene/PLA filaments with a 20/80 wt% to realize additively manufactured (AM) supercapacitor platforms (G/AMEs) fabricated via fused deposition modeling. Electrochemical decoration of the G/AMEs with MoO_2 nanowires (MoO_2-G/AMEs) is shown to be possible and is explored as a supercapacitor in 1 M H_2SO_4, and ionic liquids: 1-butyl-3-methylimidazolium hexafluorophosphate ($[C_4MIM][PF_6]$), and 1-butyl-3-methylimidazolium tetrafluoroborate ($[C_4MIM][BF_4]$). Optimization of the MoO_2-G/AMEs demonstrates supercapacitance up to 1212 F g^{-1} when used in a symmetric arrangement.

2. Results and Discussion

A full description of the G/AMEs fabrication and subsequent electrochemical decoration with MoO_2 is described within the Experimental Section with a visual description of the filament extrusion and subsequent additive manufacturing given in **Figure 1**A,B. It is important to note that the molybdenum oxides deposited via the technique described herein typically is comprised of a mixture of MoO_2 and MoO_3, it is however, common practice within the literature to denote the molybdenum oxides deposited as MoO_2.[21] Following the additive manufacturing of the G/AMEs, they were electrochemically decorated with MoO_2 using a solution of 1×10^{-3} M Na_2MoO_4 (in 1 M NaCl and 1 M NH_4Cl adjusted to pH 8.5 with liquid NH_3) at variable potential voltages and time spans. Using cyclic voltammetry (CV), the electrochemical potential was swept from +0.5 to –1.5 V (vs Ag/AgCl) where the electrochemical deposition of MoO_2 onto the electrode surface was observed as an electrochemical reduction peak at –1.25 V (vs Ag/AgCl). In this electrochemical process, the reduction of Mo^{6+} to Mo^{4+} occurs through the following reaction mechanism: $MoO_4^{2-} + 2H_2O + 2e^- \rightarrow MoO_2 + 4OH^-$, resulting in the electrochemical decoration of MoO_2 deposited on the surface of the AM electrodes with the subsequent electrodes being denoted as MoO_2-G/AMEs. Note that in the experiments performed herein, the potential at which the

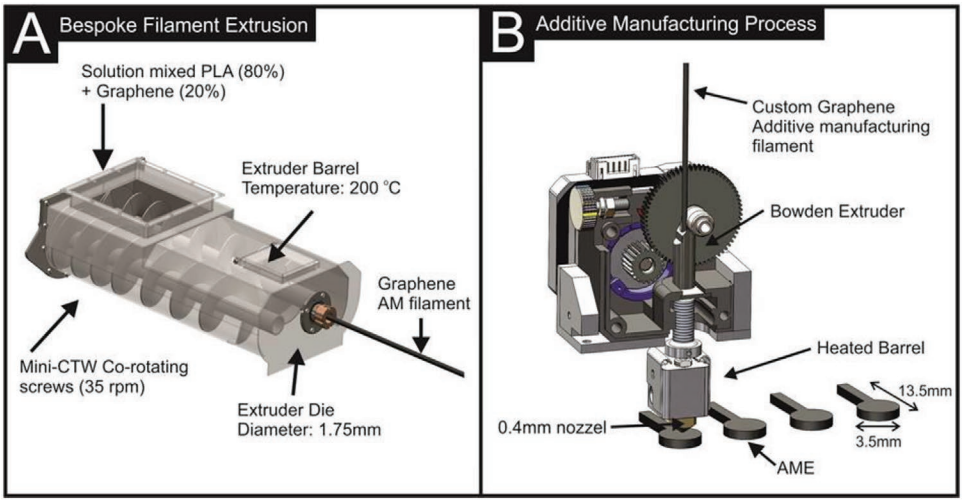

Figure 1. The manufacturing methodology of the G/AMEs, A) the powder feedstock of graphene solution mixed into PLA polymer is extruded by a Thermo MiniCTW twin screw extruder into a filament of ≈1.75 mm in diameter, B) the resulting filament is additively manufactured (fused deposition modeling) into "tabs" of standardized dimensions.

MoO_2 electrodeposition occurs is ≈–1.25 V, which is not too dissimilar to other reports using highly ordered pyrolytic graphite (HOPG)[22] and graphitic screen-printed electrodes (SPEs),[21] given the differing composition of the G/AMEs. The MoO_2-G/AMEs were fabricated using chronoamperometry with exploring the deposition potential (–1.4/–1.6 V (vs Ag/AgCl)) and time (600/300 s) which are then explored toward their ability to act as supercapacitive devices.

The capacitive characterization of the MoO2-G/AMEs was performed initially using CV and galvanostatic charge–discharge (GCD) within three different electrolytes: 1.0 M H_2SO_4 and two nonaqueous solutions of room temperature ionic liquid (RTIL) [C_4MIM][PF_6] and [C_4MIM][BF_4]. The utilization of RTILs as an electrolyte is a common strategy employed in the development of novel supercapacitors due to their reported benefits that include: wide operational electrochemical (voltage) window, high electrical conductivity, practically zero or negligible volatility, high electrical and ionic conductivity, thermal stability, favorable solvating properties, and relative environmental resilience.[23] Such properties allow for consistent performance of the devices, over a broad range of applications and environmental conditions, without significant modification or expenditure. The reason we chose to explore aqueous media and ionic liquids is due to the latter providing substantial benefits over that of the former. While ionic liquids have a range of benefits (see above), the main advantage in the case of supercapacitors is their wide and stable potential range. In the simplest sense, the specific energy, E, of a capacitor has the relationship: $E = 1/2C\Delta V^2$, where ΔV is the potential difference (potential window), and C is the capacitance. Thus, the maximum energy that can be stored in a capacitor device depends on ΔV^2. In the case of aqueous-based media, the accessible potential window is limited due to the decomposition of water resulting in unsatisfactory energy density outputs.[24] Thus, the wide accessible electrochemical window of ionic liquids allows an increase in the energy output with up to 4.5 V reported[25] which, using the equation above, translates to ≈20-fold increase in energy storage over that of an aqueous media electrolyte.

In this paper, we first consider the CV responses of the G/AMEs and the MoO_2-G/AMEs using a two-electrode symmetrical system, where both the electrodes are identical in form and modifications, chosen for simplicity, repeatability, and future ease of fabrication of a complete AM free-standing supercapacitor device. The analysis is carried out in H_2SO_4, [C_4MIM][PF_6], and [C_4MIM][BF_4]. CV was performed with typical responses shown in **Figure 2**A for the G/AMEs and the MoO_2-G/AMEs in [C_4MIM][BF_4] over the windows –2.0 to +2.0 V and –4.0 to +4.0 V demonstrating that the optimal supercapacitance is within the range of –4.0 to +4.0 V window. In Figure 2A, we can see that the modification and the introduction of the MoO_2 significantly increase the capacitance of the CV, however unlike in previous studies there seems to be no detrimental alteration in the obtained oxidation and reduction peaks, in fact there is a slight increase in the achievable peak currents. The capacitance is likely due to the primary electrochemical process of H^+ ion intercalation and de-intercalation at the surface (and bulk) from the following process: $MoO_2 + H^+ + e^- \rightleftarrows MoO_2^-H^+$ accompanied by double layer charging. Note that the ionic liquids are aprotic and the source of protons will come from water, which is well known to be present in ionic liquids when used "as is." Using scan rates of 1, 100, and 500 mV s^{-1}, the capacitances are calculated using equation

$$C_{cv} = \frac{\int_{V_1}^{V_2} I(V)\,dV}{(2\Delta V)(v)(m)} \quad (1)$$

where C_s is the specific capacitance exhibited by the working electrode in Faradays per gram (F g^{-1}), V_1 and V_2 are the potential limits of the voltammogram essentially ΔV is the potential difference between V_2 and V_1 in volts (V), v is the voltammetric scan rate (V s^{-1}), and m is the material (MoO_2) mass in grams. The determined capacitance values are shown in **Table 2**. The specific capacity is shown to be inversely proportional to the scan rate, which is due to ions, at lower scan rates, penetrating

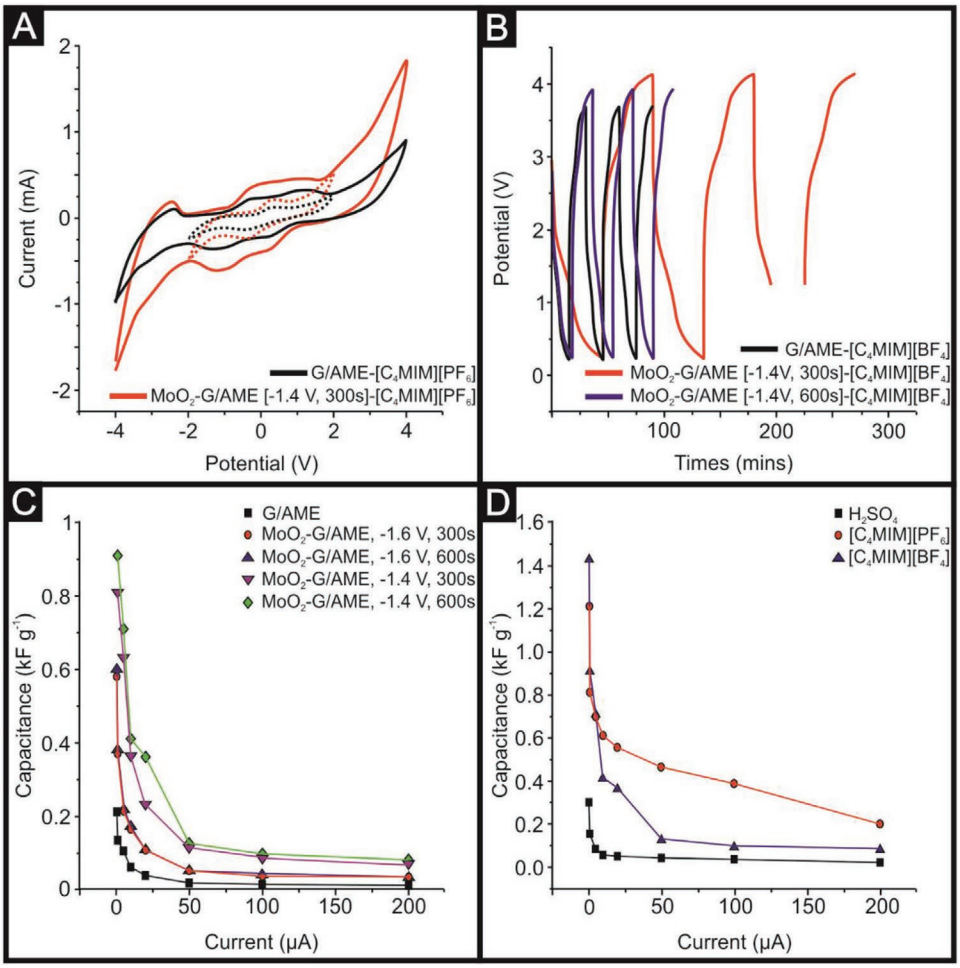

Figure 2. A) Cyclic voltammetric profiles of MoO_2-G/AMEs and G/AMEs recorded in $[C_4MIM][BF_4]$. B) The first three cycles of the MoO_2-G/AMEs and G/AMEs (both 300 s, respectively), in $[C_4MIM][BF_4]$. C) The capacitive performance of the G/AMEs and the MoO_2-G/AMEs over extended current ranges from 1 to 200 μA. D) The capacitive performance of the MoO_2-G/AMEs (–1.4 V, 600 s) in each of the tested electrolytes.

deeper inside the electrode material leading to a better surface coverage, with the $[C_4MIM][BF_4]$ electrolyte demonstrating consistently the highest performance for each electrode pair. Table 2 also shows a comparison of the unmodified G/AME, and MoO_2-G/AMEs clearly demonstrating the electrochemical decoration improve the capacitance.

GCD tests can also be used to evaluate the performance of the supercapacitors, these being the preferred method for DC testing. The GCD process is measured by the responsive potential with respect to time unlike CV, which evaluates data correlating with electrochemical phenomena arising at the electrode/electrolyte interface. The GCD measurement is completed in two steps: 1) a constant current charges a supercapacitor first, and then 2) the supercapacitor is discharged in a specific voltage range or charge/discharge time. Capacitive analysis of GCD was performed using a symmetrical two-electrode approach, such as the one described above (an electrode spacing of 5 mm was utilized). Figure 2B shows three charge/discharge cycles of the G/AME again, utilizing the –1.4 V deposition potential held for 300 and 600 s to produce the G/AME-MoO_2. The capacitance of the systems was calculated using Equation (1) where the well-documented correlation between current and capacitance is again observed, as shown in Figure 2C,D where high currents are observed to reduce the capacitance. In this case, the reduction is significant and results in an order of magnitude change in the performance, this is largely due to the filler quantity of the electrode and the relatively high resistance having a significant impact on the performance at the higher currents. Of note, Figure 2C shows the comparison of the G/AME with that of different electrochemical modification strategies (potential and time) where the MoO_2-G/AMEs prepared by –1.4 V, 600 s give rise to the optimal capacitive response. Last, Figure 2D compares the

Table 2. Capacitative (F g^{-1}) performance of the G/AMEs and MoO_2-G/AMEs in differing electrolytes: 1 M H_2SO_4, $[C_4MIM][PF_6]$, and $[C_4MIM][BF_4]$. The electrodes utilized here were fabricated using the optimal electrochemical decoration parameters (–1.4 V, 600 s).

	H_2SO_4			$[C_4MIM][PF_6]$			$[C_4MIM][BF_4]$		
Scan rate (mV s^{-1})	1	100	500	1	100	500	1	100	500
G/AMEs	112	89.1	1.21	213	75.8	34.7	276	113	87.3
MoO_2-G/AMEs	142	14.1	11.2	1010	807	234	1212	342	119

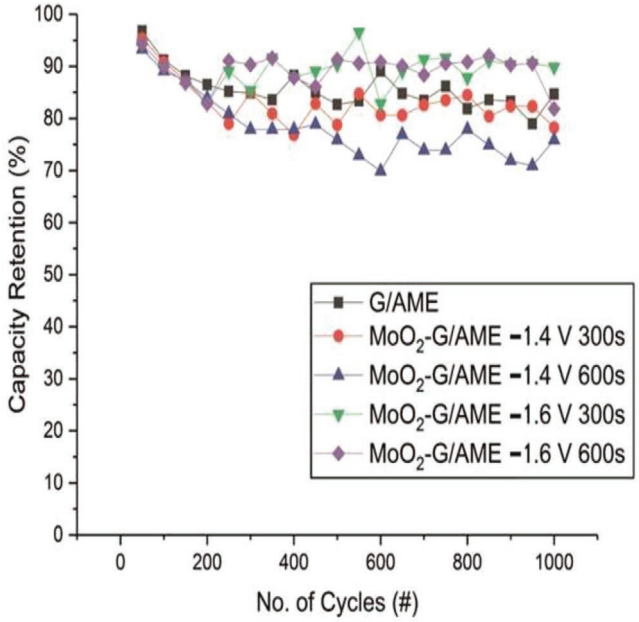

Figure 3. A) Capacity retention of the G/AME and modified MoO_2-G/AME supercapacitors, using an electrolyte of $[C_4MIM][BF_4]$, showing a similar capacity retention over 1000 cycles regardless of the modification carried out on the surface (vs Ag/AgCl).

capacitance for the three electrolytes, 1 M H_2SO_4, $[C_4MIM][PF_6]$, and $[C_4MIM][BF_4]$ and are summarized within Table 2 where significant improvements are observed when using ionic liquids over that of conventional aqueous media. The inspection of Table 1 shows that the improved capacitance in ionic liquid is due to the wider electrochemical window that is not possible in the aqueous media. The capacitance output of the MoO_2-G/AMEs is compared to prior literature which demonstrates an excellent performance of 1212 F g^{-1} (@1.48 A g^{-1}). Note that the various electrolyte and cell configurations do not allow direct comparisons to be feasibly made. Furthermore, the capacitive stability was explored via 1000 GCD cycles, with the resultant plots being shown in **Figure 3**. It can be seen that the consistency of performance of the devices remains, in the most part, over 80%, with the one exception being the MoO_2 modification at −1.4 V for 300 s, indicating there is a potentially less direct binding to the surface, and the MoO_2 is liberated from the surface during testing. It should be noted that all electrodes perform similarly to the unmodified G/AMEs, indicating that there is no inherent loss in cycling reliability after the surface modification is made. Overall, the optimal electrochemical decoration in terms of capacitive output and stability is clearly the electrochemical decoration of MoO_2 using a potential of −1.4 V held at 600 s.

Scanning electron microscope (SEM) images are shown in **Figure 4** of the G/AMEs and MoO_2-G/AMEs where it is clear from Figure 4C that MoO_2 nanowires-type structures are formed on the edge planes of the graphitic structures in G/AMEs. In this case, the nanostructures form at points that the graphene filler extrudes from the polymer matrix. The structures were predominantly concentrated, although not exclusively, around the edge structures. The contrasting conductivity of the polymer matrix and the graphitic surface structures onto which the MoO_2 deposition takes place cause highly localized points of charge build up during SEM analysis, resulting in a limitation to the detail we are able to obtain. Further characterization was performed using X-ray photoelectron spectroscopy (XPS) to determine the composition of the electrochemically decorated structures. The obtained XPS spectrum shown in **Figure 5**B reveals that the surface regions of the synthesized electrodes are composed of Mo, O, and C atoms. Figure 5A,B shows the spectrum for the MoO_2-G/AMEs with an electrodeposition procedure of −1.4 V for 600 s. The Mo 3d XPS spectrum shows four peaks, the stronger peaks at 235.8 and 232.5 eV are assigned to Mo $3d_{3/2}$ and Mo $3d_{5/2}$ of the Mo^{6+} due to partial oxidation of the surface MoO_2 in air. The detected atomic composition of Mo, O, and C is 3.40%, 56.31%, and 39.91%, respectively, indicating the relatively low concentration of the Mo present on the surface as it is only a surface modification appearing at graphitic features on the AM electrode surface. To confirm that the modification of the electrodes has no negative or unwanted effects on the electrode composition other than surface modification, a depth profile was obtained for the modified G/AMEs. The MoO_2-G/AMEs surface is etched using the Ar^+ high flux minibeam of the XPS, which allows us to penetrate the surface of the MoO_2-G/AMEs, layer by layer. This approach allows for the complete and accurate characterization

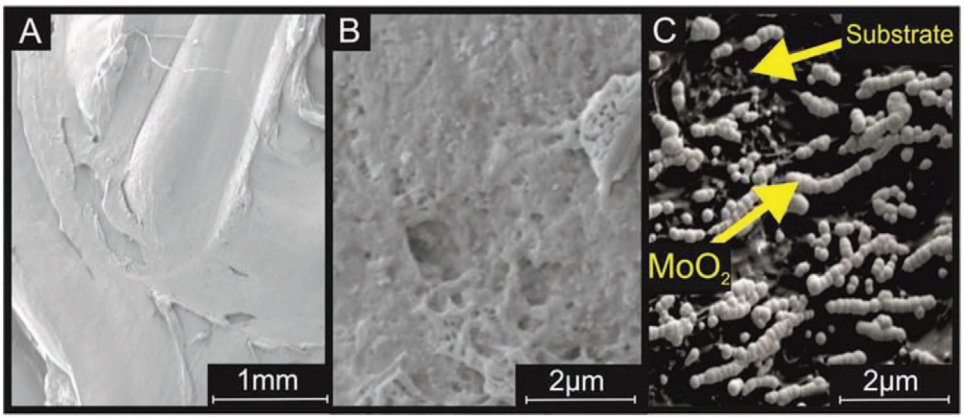

Figure 4. SEMs of A,B) the G/AME and C) MoO_2-G/AME. Electrochemical decoration parameters: −1.4 V, 600 s.

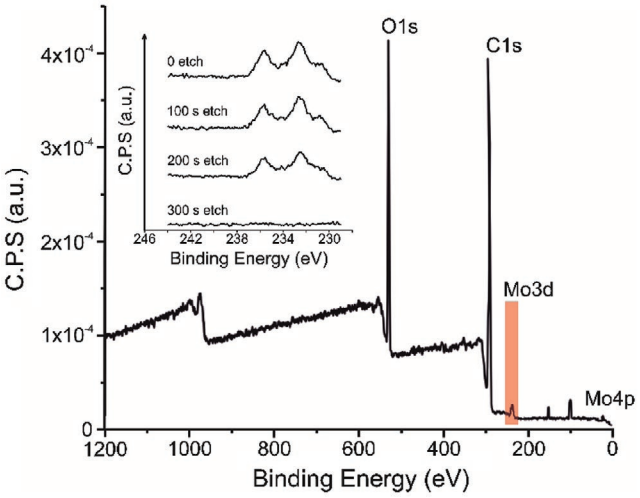

Figure 5. Overall XPS spectra of the MoO_2-G/AMEs. Electrochemical decoration parameters: –1.4 V, 600 s. Inset: XPS of the MoO_2-G/AMEs, showing the presence of MoO_2 oxides after 0–300 s etching from the surface of the electrode. This indicates that the electrochemical decoration is surface bound only.

of the surface material and ensures that there is no effect of the bulk composition. Figure 5A,B shows the Mo 3d XPS spectra for MoO_2-G/AMEs with an electrodeposition procedure of –1.4 V for 600 s. The Mo peaks appear as present and consistent with 0 to 200 s of etching, however after 300 s of etching the presence of the Mo peaks is completely removed. This indicates that the surface modification is acting exactly as expected, with the MoO_2 nanostructures forming around graphitic features upon the G/AMEs surface, without any unwanted permeation into the electrodes structure or unwanted chemical or morphological changes to the AMEs. This allows us to provide a direct comparison to previous studies of G/AMEs for energy storage without any further consideration of the chemical influence of the structure of the G/AMEs.

3. Conclusions

This paper represents the first use of a post-printing electrochemical modification methodology upon graphene-based AM electrodes in order to enhance their capacitive properties. Optimizing the conditions for MoO_2 nucleation upon the surface of a G/AME allowed us to fabricate highly efficient supercapacitors (G/AME-MoO_2) that displayed significantly greater capacitance than a bare/unmodified G/AME. Given that AM, as a method to produce electrode materials, is still in its infancy when compared to more well-established mass producible techniques such as screen-printing or roll-to-to printing, it has the potential to fill a useful and currently unexploited niche, in that it can create electrodes in complex 3D geometries and compositions that were previously unfeasible. This work also shows that these bespoke fabricated graphene filaments used to AM the electrochemical platform can be used as a template for future decoration of other metals/metal oxide where the edge plane sites can provide nanowire templates. Future work could also be extended to other additive manufacturable plastics in the fabrication of bespoke graphene-based additive manufactured electrodes (e.g., ABS) and the electrochemical platform can be further extended through intelligent additive manufactured design and fabrication. The MoO_2-G/AMEs described herein as well as the decoration technique utilized in their creation, represents a significant enhancement in unlocking AMs potential as a valid manufacturing route for device level supercapacitor architectures.

4. Experimental Section

Chemicals: All chemicals used were of an analytical grade and used without any further purification from Sigma-Aldrich (UK) unless stated otherwise. The ionic liquids were purchased and used as received: $[C_4MIM][PF_6]$ and $[C_4MIM][BF_4]$. The solutions were prepared with deionized water of resistivity not less than 18 MΩ cm. Electrochemical measurements were carried out at room temperature using an Autolab PGSTAT302N (Metrohm, UK).

Additive Manufactured Graphene Electrodes (G/AMEs): Graphene-based composites were fabricated by pre-mixing graphene and PLA utilizing a facile solution-based mixing step. The utilization of PLA instead of other commonly used polymers was largely due to the lower melting temperature when compared to other commonly used materials in additive manufacturing, such as ABS or PET. This involved the graphene being dispersed within O-xylene by sonication for 30 min, and heated under reflux to 160 °C, the PLA was then added to the mixture and left for 3 h. The resulting homogenous (solution phase) mixture was then recrystallized within methanol, filtered, and left to dry (at 50 °C within a fan oven) until any remaining O-xylene had evaporated. The resulting graphene-loaded PLA powder mix was then extruded with a Thermo MiniCTW twin-screw extruder (ThermoScientific, UK) at a temperature of 200 °C and a screw speed of 20 rpm. The filament diameter was set by a combination of the die, which was drilled to 1.75 mm, and the draw off speed was monitored manually. The resulting filament was of diameter 1.76 ± 0.1 mm. The additive designs were drawn using 3DS's Solidworks, and were printed utilizing either a filament deposition modeling (FDM) 3D printer (ZMorph, Warsaw, Poland), using a custom drilled 1.0 mm diameter nozzle to prevent blockages or a stereolithography (SLA) printer (Form 2, Formlabs, USA). In this paper, all additively manufactured electrodes were 20% wt of graphene nanoplatelets (NP25b1, Graphene Industries, UK) in a PLA matrix. Throughout this material was simply referred to as graphene. This was comprised of obtaining the most amount of active material, yet still being reliably constructed by AM. Using the near-ideal outer-sphere redox probe, 1×10^{-3} M hexaammineruthenium (III) chloride/0.1 M KCl, the heterogenous electron transfer rate constant, k^0, was determined.[26] The k^0 was found to correspond to 7.2×10^{-3} cm s^{-1}. This was an order of magnitude bigger than commercially available filament.[27]

Additive Manufactured Graphene Electrodes Electrochemically Decorated with MoO_2 (G/AME-MoO_2): Previous reports indicated that MoO_2 selectively deposited upon the available edge plane like-site/defects of HOPG and SPEs.[21,22b] Electrochemical decoration of the G/AMEs electrodes took place via a chronoamperometric methodology following previous reports which indicated that MoO_2 selectively deposited upon the available edge plane like-site/defects of HOPG, SPEs, and pristine graphene.[21,22b,28] The G/AMEs were modified similarly by holding the potential at the chosen values for different times in 1×10^{-3} M Na_2MoO_4 (in 1 M NaCl and 1 M NH_4Cl adjusted to pH 8.5 with liquid NH_3) in order to electrochemically deposit MoO_2 onto the G/AME. The solution was comprised of: 1×10^{-3} M Na_2MoO_4 (in 1 M NaCl and 1 M NH_4Cl adjusted to pH 8.5 with liquid NH_3) as previously reported where screen-printed electrodes were decorated with MoO_2 but no supercapacitor studies were reported in this prior reference.[23]

Equipment: Capacitance and voltammetric measurements were performed using an "Autolab–μAutolab Type III" (Metrohm Autolab,

The Netherlands) potentiostat. All capacitance measurements reported herein were performed utilizing a symmetrical electrochemical set-up. Note the electrode spacing utilized was 5 mm. Three-electrode configuration (half-cell) was used for the electrochemical decoration of the G/AME, where the G/AMEs were the working electrode, a nickel wire counter/auxiliary electrode and a silver/silver chloride electrode (Ag/AgCl) reference electrode completed the circuit. SEM images and surface element analysis were obtained with a JEOL JSM 5600LV model having energy-dispersive X-ray microanalysis package. XPS characterization was carried out utilizing the Kratos AXIS Supra+ with depth profiling Minibeam 4 high flux monoatomic Ar+ ion source and an X-ray power source of 225.00 W. An aluminium filament was used with an emission current of 15.00 mA.

Acknowledgements

Funding from the Engineering and Physical Sciences Research Council (Reference: EP/N001877/1) is acknowledged.

Conflict of Interest

The authors declare no conflict of interest.

Data Availability Statement

Research data are not shared.

Keywords

additive manufacturing, graphene additive manufacturing, ionic liquids, MoO_2, supercapacitors

Received: February 5, 2021
Revised: April 9, 2021
Published online:

[1] a) S. H. Huang, P. Liu, A. Mokasdar, L. Hou, *Int. J. Adv. Manuf. Technol.* **2013**, *67*, 1191; b) M. Vaezi, H. Seitz, S. Yang, *Int. J. Adv. Manuf. Technol.* **2013**, *67*, 1721; c) J. Czyżewski, P. Burzyński, K. Gaweł, J. Meisner, *J. Mater. Process. Technol.* **2009**, *209*, 5281.

[2] a) P. L. D. Santos, S. J. Rowley-Neale, A. G. M. Ferrari, J. A. Bonacin, C. E. Banks, *ChemElectroChem* **2019**, *6*, 5633; b) J. P. Hughes, P. L. d. Santos, M. P. Down, C. W. Foster, J. A. Bonacin, E. M. Keefe, S. J. Rowley-Neale, C. E. Banks, *Sustainable Energy Fuels* **2020**, *4*, 302.

[3] a) D. Espalin, D. W. Muse, E. MacDonald, R. B. Wicker, *Int. J. Adv. Manuf. Technol.* **2014**, *72*, 963; b) S. J. Leigh, R. J. Bradley, C. P. Purssell, D. R. Billson, D. A. Hutchins, *PLoS One* **2012**, *7*, e49365.

[4] a) R. Kötz, M. Carlen, *Electrochim. Acta* **2000**, *45*, 2483; b) D. Qu, *J. Power Sources* **2002**, *109*, 403.

[5] C. Costentin, T. R. Porter, J.-M. Savéant, *ACS Appl. Mater. Interfaces* **2017**, *9*, 8649.

[6] C. W. Foster, M. P. Down, Y. Zhang, X. Ji, S. J. Rowley-Neale, G. C. Smith, P. J. Kelly, C. E. Banks, *Sci. Rep.* **2017**, *7*, 42233.

[7] M. P. Down, E. Martínez-Periñán, C. W. Foster, E. Lorenzo, G. C. Smith, C. E. Banks, *Adv. Energy Mater.* **2019**, *9*, 1803019.

[8] Y. Li, F. Tang, R. Wang, C. Wang, J. Liu, *ACS Appl. Mater. Interfaces* **2016**, *8*, 30232.

[9] J. Rajeswari, P. S. Kishore, B. Viswanathan, T. K. Varadarajan, *Electrochem. Commun.* **2009**, *11*, 572.

[10] P. Ju, Z. Zhu, X. Shao, S. Wang, C. Zhao, X. Qian, C. Zhao, *J. Mater. Chem. A* **2017**, *5*, 18777.

[11] T. Zhang, L.-B. Kong, M.-C. Liu, Y.-H. Dai, K. Yan, B. Hu, Y.-C. Luo, L. Kang, *Mater. Des.* **2016**, *112*, 88.

[12] Y. Ma, Y. Jia, L. Wang, M. Yang, Y. Bi, Y. Qi, *J. Mater. Chem. A* **2016**, *4*, 10414.

[13] H. Si, L. Sun, Y. Zhang, L. Wu, Y. Zhang, Y. Zhang, *Dalton Trans.* **2020**, *49*, 1637.

[14] Y. Tian, H. Du, M. Zhang, Y. Zheng, Q. Guo, H. Zhang, J. Luo, X. Zhang, *J. Mater. Chem. C* **2019**, *7*, 9545.

[15] J. Tian, H. Zhang, Z. Li, *ACS Appl. Mater. Interfaces* **2018**, *10*, 29511.

[16] L. Zhang, H. Lin, L. Zhai, M. Nie, J. Zhou, S. Zhuo, *J. Mater. Res.* **2017**, *32*, 292.

[17] a) C. An, Y. Zhang, H. Guo, Y. Wang, *Nanoscale Adv.* **2019**, *1*, 4644; b) H. Jiang, L. Yang, C. Li, C. Yan, P. S. Lee, J. Ma, *Energy Environ. Sci.* **2011**, *4*, 1813; c) M. A. A. M. Abdah, N. H. N. Azman, S. Kulandaivalu, Y. Sulaiman, *Mater. Des.* **2020**, *186*, 108199; d) V. Sharma, I. Singh, A. Chandra, *Sci. Rep.* **2018**, *8*, 1307.

[18] a) C. Jian, Q. Cai, W. Hong, J. Li, W. Liu, *Small* **2018**, *14*, 1703798; b) M. P. Minimol, K. P. Rao, S. Y. Ram, K. Vidyasagar, *Int. J. Chem. Soc.* **2003**, *115*, 419; c) A. Hashemzadeh, R. Ahmadi, D. Yarali, N. Sanaei, *Mater. Res. Express* **2020**, *6*, 1250d3.

[19] P. Ju, Z. Zhu, X. Shao, S. Wang, C. Zhao, X. Qian, C. Zhao, *J. Mater. Chem. A* **2017**, *5*, 18777.

[20] J.-Z. Wu, X.-Y. Li, Y.-R. Zhu, T.-F. Yi, J.-H. Zhang, Y. Xie, *Ceram. Int.* **2016**, *42*, 9250.

[21] S. J. Rowley-Neale, D. A. C. Brownson, C. E. Banks, *Nanoscale* **2016**, *8*, 15241.

[22] a) E. C. Walter, M. P. Zach, F. Favier, B. J. Murray, K. Inazu, J. C. Hemminger, R. M. Penner, *ChemPhysChem* **2003**, *4*, 131; b) T. J. Davies, M. E. Hyde, R. G. Compton, *Angew. Chem.* **2005**, *44*, 5121.

[23] a) M. C. Buzzeo, R. G. Evans, R. G. Compton, *ChemPhysChem* **2004**, *5*, 1106; b) A. Eftekhari, *Energy Storage Mater.* **2017**, *9*, 47; c) S. Shahzad, A. Shah, E. Kowsari, F. J. Iftikhar, A. Nawab, B. Piro, M. S. Akhter, U. A. Rana, Y. Zou, *Global Challenges* **2019**, *3*, 1800023.

[24] S. Sun, J. Lang, R. Wang, L. Kong, X. Li, X. Yan, *J. Mater. Chem. A* **2014**, *2*, 14550.

[25] A. Balducci, R. Dugas, P. L. Taberna, P. Simon, D. Plée, M. Mastragostino, S. Passerini, *J. Power Sources* **2007**, *165*, 922.

[26] A. García-Miranda Ferrari, C. W. Foster, P. J. Kelly, D. A. C. Brownson, C. E. Banks, *Biosensors* **2018**, *8*, 53.

[27] C. W. Foster, M. P. Down, Y. Zhang, X. Ji, S. J. Rowley-Neale, G. C. Smith, P. J. Kelly, C. E. Banks, *Sci. Rep.* **2017**, *7*, 42233.

[28] A. García-Miranda Ferrari, C. W. Foster, D. A. C. Brownson, K. A. Whitehead, C. E. Banks, *Sci. Rep.* **2019**, *9*, 12814.